

Baltimore Atlas: FreqWeaver Adapter for Semi-supervised Ultra-high Spatial Resolution Land Cover Classification

Junhao Wu
jwu17@students.towson.edu
Towson University
Towson, MD, USA

Aboagy-Ntow Stephen
saboagy1@students.towson.edu
Towson University
Towson, MD, USA

Chuyuan Wang
cwang@towson.edu
Towson University
Towson, MD, USA

Gang Chen
Gang.Chen@charlotte.edu
University of North Carolina at
Charlotte
Charlotte, NC, USA

Xin Huang
xhuang@towson.edu
Towson University
Towson, MD, USA

ABSTRACT

Ultra-high Spatial Resolution Land Cover Classification is essential for fine-grained land cover analysis, yet it remains challenging due to the high cost of pixel-level annotations, significant scale variation, and the limited adaptability of large-scale vision models. Existing methods typically focus on 1-meter spatial resolution imagery and rely heavily on annotated data, whereas practical applications often require processing higher-resolution imagery under weak supervision. To address this, we propose a parameter-efficient semi-supervised segmentation framework for 0.3 m spatial resolution imagery, which leverages the knowledge of SAM2 and introduces a remote sensing-specific FreqWeaver Adapter to enhance fine-grained detail modeling while maintaining a lightweight design at only 5.96% of the total model parameters. By effectively leveraging unlabeled data and maintaining minimal parameter overhead, the proposed method delivers robust segmentation results with superior structural consistency, achieving a 1.78% improvement over existing parameter-efficient tuning strategies and a 3.44% gain compared to state-of-the-art high-resolution remote sensing segmentation approaches.

CCS CONCEPTS

• **Computing methodologies** → **Computer vision; Image segmentation; Semi-supervised learning; Transfer learning; Convolutional neural networks.**

KEYWORDS

High-resolution remote sensing, Semi-supervised segmentation, Large model priors, Small object segmentation, Structural consistency

1 INTRODUCTION

High-precision segmentation of remote sensing (RS) imagery serves as a cornerstone in a wide range of real-world applications, including land cover classification, urban planning, environmental monitoring, and disaster response [6, 26]. With the advent of ultra-high-resolution (UHR) imagery—particularly at the 0.3-meter ground sampling distance—RS data now enables significantly richer spatial detail, allowing for the identification of fine-scale urban features such as vehicles, street furniture, residential swimming pools, and

narrow alleyways [5]. This spatial granularity facilitates parcel-level land use analysis and fine-grained urban modeling, thereby unlocking new frontiers for RS research and practical applications [23].

However, the transition to UHR imagery introduces substantial challenges for semantic segmentation models. While existing approaches demonstrate robust performance on datasets with 1-meter resolution, their effectiveness often deteriorates when applied to finer resolutions such as 0.3 meters [29, 31, 50]. The increased level of detail exacerbates the complexity of capturing fine-grained structural boundaries and contextually diverse object classes [16]. Effective segmentation at this scale requires models capable of simultaneously modeling local geometry and global semantics, motivating the development of novel architectures tailored to the intricacies of UHR data.

Moreover, a major bottleneck in the advancement of ultra-high-resolution (UHR) RS segmentation lies in the reliance on large-scale, pixel-wise annotated datasets for fully supervised training [25]. While effective under ideal settings, manual annotation of ultra-high-resolution RS imagery is prohibitively time-consuming and labor-intensive, limiting the scalability and practical deployment of such models [9]. Moreover, when operating under limited supervision, these models often exhibit performance degradation and poor generalization across diverse scenes and geographies [49].

Recently, the emergence of pre-trained foundation models such as the Segment Anything Model (SAM) [20, 36] has demonstrated strong generalization capabilities across diverse visual tasks. Trained on extensive image-mask pairs, SAM2 [36] encapsulate transferable semantic priors and offer a promising path toward alleviating annotation dependency via transfer learning on downstream tasks like high-resolution RS image segmentation [48].

Although full fine-tuning of foundation models can enhance performance, it also incurs substantial computational and memory overheads [7]. Parameter-Efficient Fine-Tuning (PEFT) methods, such as Adapters [10] and Low-Rank Adaptation (LoRA) [11], have emerged as viable alternatives for resource-conscious adaptation. However, due to the pronounced domain gap between the natural or medical images used for pre-training and the unique characteristics of RS data, conventional PEFT strategies often fail to generalize well in RS scenarios [19, 38]. Moreover, remote sensing imagery encompasses a wide spectrum of object scales—from large-scale vegetated

regions to fine-grained human-made structures—necessitating robust multi-scale feature modeling capabilities [2].

To this end, we propose *FreqWeaver*, a frequency-temporal modulation adapter designed to enhance the adaptability of foundation models like SAM2 to ultra-high-resolution (UHR) remote sensing imagery. *FreqWeaver* decomposes input features into low- and high-frequency components via spectral filtering, which are then processed using large and small receptive field convolutions to respectively capture global semantics and fine-grained structures. A spatial-domain residual branch is further incorporated to complement missing local details. This design not only leverages the semantic priors encoded in SAM2 for basic object recognition, but also enhances the model’s capacity to represent diverse spatial patterns in UHR data. In particular, the proposed multi-scale feature interaction mechanism significantly improves the model’s ability to delineate fine boundary details of large-scale objects and accurately identify small, morphologically complex structures—thereby enabling precise and robust segmentation across heterogeneous geographic scenes under strict parameter constraints.

Remote sensing (RS) systems, owing to their extensive spatial coverage and high temporal resolution, continuously collect vast amounts of unlabeled imagery, offering a rich yet underutilized resource for semi-supervised learning (SSL) [46]. To address the challenges posed by limited supervision and high annotation costs in high-resolution RS segmentation, we propose a semi-supervised fine-tuning framework built upon a pre-trained foundation model. The framework integrates a teacher–student consistency learning paradigm with an uncertainty-aware weighting strategy, enabling efficient and robust domain adaptation. By dynamically modulating the contribution of pseudo-labels during training, the method effectively suppresses the adverse impact of noisy supervision—an issue particularly prevalent in RS imagery due to complex backgrounds, ambiguous boundaries, and high inter-class similarity. As a result, it significantly enhances model robustness and generalization across diverse geographic regions, acquisition conditions, and sensor types [4], while simultaneously reducing reliance on costly manual annotations.

The main contributions of this paper are summarized as follows:

- **PEFT-Driven Semi-Supervised Tuning of SAM2:** We propose an Adapter-based PEFT strategy integrated with an uncertainty-guided consistency regularization mechanism for the SAM2 model [36]. This approach significantly reduces the dependency on labeled data, achieving efficient segmentation performance while updating fewer than 5.96% of the total model parameters.
- **0.3m-Resolution Remote Sensing Dataset for Fine-Grained Segmentation:** To support detailed land cover analysis, we construct a high-resolution (0.3m) remote sensing dataset over Baltimore. Compared to conventional 1m-Resolution datasets, it offers finer spatial granularity and greater object diversity, providing a more challenging and representative benchmark for evaluating segmentation models under real-world urban conditions.
- **FreqWeaver Adapter for Disentangled Frequency–Temporal Multi-Scale Modeling:** To better capture the fine-grained

structures and scale-diverse patterns in high-resolution RS imagery, we introduce *FreqWeaver*, a frequency–temporal modulation adapter that decomposes features into low- and high-frequency components for separate processing via large and small receptive field convolutions. A complementary spatial-domain branch further enriches semantic representation. This design enhances SAM2’s capacity to model both global context and local detail, enabling more precise and parameter-efficient multi-scale segmentation.

- **Uncertainty-Aware Semi-Supervised Learning:** Considering the high error rates of pseudo-labels in remote sensing imagery—caused by complex backgrounds, fine-grained boundaries, and inter-class spectral similarity—we propose an uncertainty-aware semi-supervised framework that downweights unreliable predictions based on entropy. This design effectively suppresses misleading gradients from noisy supervision and improves the robustness of segmentation across diverse regions, sensors, and seasonal conditions.

2 RELATE WORK

2.1 Foundation Models in Remote Sensing

Foundation Models (FMs), notably Vision Transformer (ViT)-based architectures [3], learn transferable representations from extensive unlabeled data, enabling strong generalization across diverse tasks. Adapting FMs to remote sensing (RS) is challenging due to RS imagery’s distinct characteristics (multi-scale spatial structures, rich spectral content, complex semantic distributions) that diverge significantly from natural images.

To address these challenges, *Geospatial Foundation Models* (GeoFMs) have emerged. Models like *Clay* [32] and *Prithvi* [39], pre-trained on extensive satellite/aerial data, are optimized for Earth Observation (EO). Recent advances such as *S2MAE* (spatial-spectral pretraining) [34], *GeoChat* (vision-language grounding) [33], and *SkySense* (multi-modal integration) [35] highlight the trend towards task-adaptive geospatial architectures.

General-purpose FMs like the *Segment Anything Model (SAM)* [21] and *SAM2* [36] offer prompt-driven, class-agnostic segmentation. However, the original SAM performs suboptimally on RS imagery, showing limited semantic awareness, difficulty with small/dense objects, and inconsistency in tasks like semantic change detection. These issues stem from its natural image bias and lack of RS domain priors.

To address these SAM limitations, *STSAMNet* [47] integrates unsupervised domain adaptation (UDA), pseudo-label refinement, and adapter layers for improved building extraction. *SCNet* [18] uses multi-scale feature fusion and semantic alignment to adapt SAM2 for semantic change detection. Prompt generation and CLIP-based supervision are also explored for semantic guidance in RS.

These adaptations show a shift from universal zero-shot inference to *domain-specialized fine-tuning*. Thus, RS is not just adopting FMs but also shaping their development. This is driven by RS challenges like scale variation, semantic ambiguity, and the need for label-efficient geospatial analysis.

2.2 Semantic Segmentation for Complex Remote Sensing

Remote sensing image segmentation faces unique challenges. Pixel-level annotation scarcity is primary, severely limiting fully supervised methods. Second, inherent multi-scale spatial heterogeneity necessitates models adept at handling drastic scale variations (small objects to vast regions). Furthermore, high inter-class similarity and significant intra-class diversity (from varying illumination, seasons, and sensors) severely test model feature discriminability.

Semi-Supervised Semantic Segmentation (SSSS) addresses annotation scarcity by leveraging abundant unlabeled data. Key SSSS strategies include consistency regularization and pseudo-labeling [1, 37, 40]. For instance, *MUCA* [43] uses a Multi-scale Uncertainty Consistency (MSUC) module and cross-teacher-student attention to address multi-scale objects and inter-class similarity, enhancing multi-layer semantic consistency and discriminability. *SegKC* [41] improves pseudo-label quality and efficiency via heterogeneous dual-network co-training with bi-directional knowledge transfer, using a lightweight network for efficient inference.

Unsupervised Domain Adaptation (UDA) addresses domain shifts in remote sensing data, often from varying sensors or locations. For example, *STSAMNet* [47] combines UDA with the Segment Anything Model (SAM) via an adapter, optimizing segmentation for target-domain high-resolution imagery and mitigating performance drops in new regions.

While SSSS and UDA methods partially address label scarcity and domain shifts, accurately segmenting complex spatial structures and multi-scale targets remains a bottleneck. Many methods struggle to capture diverse multi-scale features or introduce artifacts during pseudo-labeling and domain adaptation, especially at boundaries or in textured areas. To overcome these limitations, we explore parameter-efficient solutions that not only reduce reliance on labeled data but also enhance multi-scale representation under minimal supervision, as detailed next.

2.3 Parameter-Efficient Fine-Tuning Method

As foundation models (FMs), including geospatial variants (GeoFMs), continue to grow in size and complexity, full fine-tuning has become increasingly impractical due to high computational costs and risks such as overfitting and catastrophic forgetting. *Parameter-Efficient Fine-Tuning (PEFT)* offers a scalable alternative by adapting models through the selective update of a small subset of parameters, while keeping the majority of pre-trained weights frozen.

Several PEFT techniques have been proposed to balance efficiency and performance. *Adapter tuning*, which inserts lightweight modules into transformer layers, has been successfully applied in models like *STSAMNet* [47] for adapting SAM to high-resolution remote sensing. *Low-Rank Adaptation (LoRA)* [12] reduces parameter overhead by constraining updates to low-rank subspaces. *Prompt tuning* [17] and *prefix tuning* [24] modify task-specific behavior through learned embeddings, without altering the base model. These methods significantly reduce training cost and memory usage, and often enhance generalization by preserving pre-trained representations.

PEFT has gained traction in remote sensing. [30] benchmarked multiple PEFT methods across diverse GeoFM architectures and

Earth observation datasets, showing that PEFT can match or surpass full fine-tuning with far lower resource requirements. [8] introduced *Sensitivity-aware PEFT (SPT)*, which identifies and prioritizes task-relevant parameters for adaptation, integrating LoRA or adapters accordingly. Domain-specific approaches such as *AiRs* [14], *TEA* [13], and *Earth-Adapter* [15] further enhance transformer adaptation for Earth observation via residual-enhanced adapters.

To address key challenges in remote sensing imagery—such as large parameter overhead, aliasing artifacts, and significant object-scale variability—we propose a novel adapter architecture that combines frequency-domain decomposition with specialized convolutional processing. By disentangling high- and low-frequency components through dedicated convolutional branches and incorporating temporal information, the proposed method enables effective multi-scale adaptation while maintaining minimal parameter cost.

3 METHOD

We propose a semi-supervised, parameter-efficient fine-tuning framework built upon the Segment Anything Model 2 (SAM2), which effectively leverages the prior knowledge of large-scale foundation models. To this end, we introduce the FreqWeaver Adapter—a lightweight yet effective module that adapts SAM2 to remote sensing data while maintaining high parameter efficiency. In addition, we design a semi-supervised learning strategy that fully utilizes unlabeled data to improve domain adaptation and generalization under limited supervision. The overall framework is illustrated in Figure 1.

3.1 FreqWeaver: Frequency-Modulated Adapter for Efficient RS Fine-Tuning

Remote sensing (RS) imagery is typically characterized by significant scale variation, densely distributed objects, and complex textures. These properties pose challenges not only to general-purpose vision models such as SAM, but also to existing parameter-efficient tuning methods, which often struggle to adapt to such complex data distributions. To address this, we propose **FreqWeaver**, a lightweight frequency-temporal modulation adapter. FreqWeaver explicitly decomposes input features into low- and high-frequency components, which are processed separately using convolutional filters with distinct receptive fields to model global semantics and fine-grained details, respectively. In addition, a temporal branch is introduced to capture residual semantic information that may not be effectively represented in the frequency domain. This design significantly improves the adaptability and structural representation capability of SAM on RS imagery, while maintaining parameter efficiency. An overview of the proposed adapter is illustrated in Figure 2.

3.1.1 Spectral Decomposition. To facilitate frequency-aware feature refinement, we perform spectral decomposition on the encoder outputs using the 2D Discrete Fourier Transform (DFT). This allows explicit separation of low- and high-frequency information for targeted processing.

Before applying the DFT, we first reshape the input feature tensor from $\mathbf{X} \in \mathbb{R}^{B \times H \times W \times C}$ to $\mathbf{X}' \in \mathbb{R}^{B \times C \times H \times W}$ to align with the channel-wise Fourier transform convention.

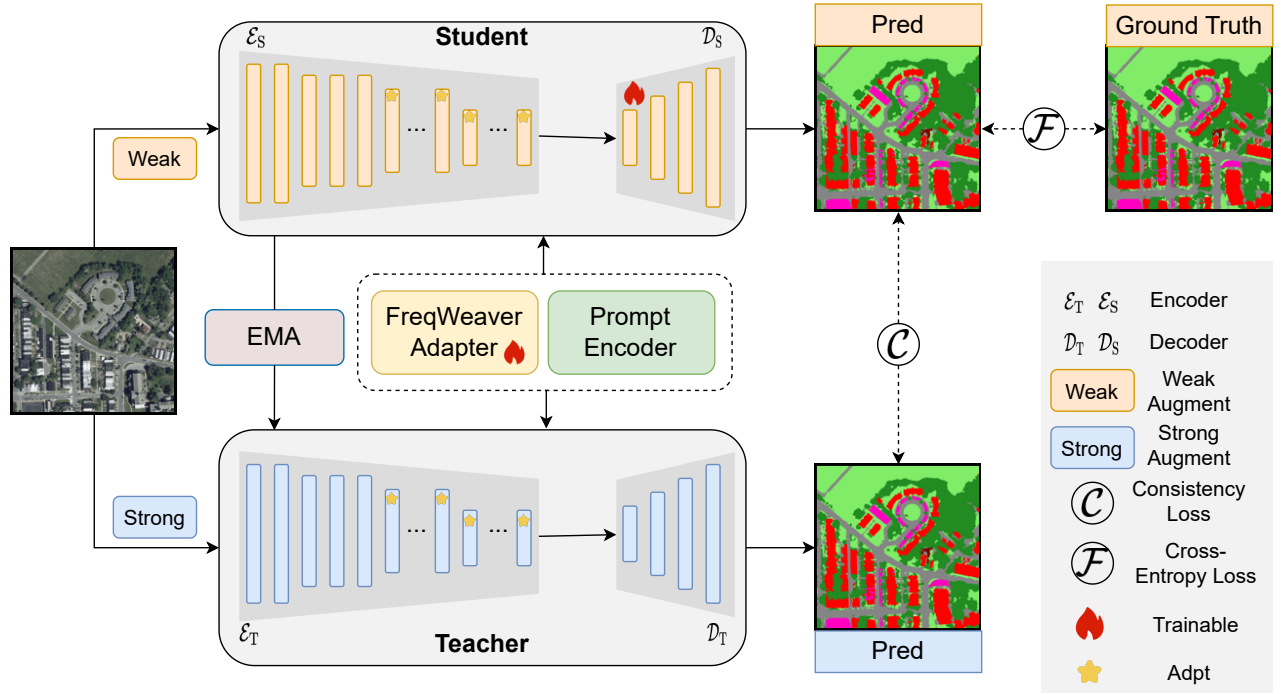


Figure 1: Overview of the proposed framework.

We then apply the 2D DFT independently to each channel as:

$$\mathbf{X}_f = \mathcal{F}_{\text{DFT}}(\mathbf{X}'), \quad (1)$$

where \mathcal{F}_{DFT} denotes the 2D Fourier transform along the spatial dimensions (H, W) for each channel. The resulting spectrum $\mathbf{X}_f \in \mathbb{C}^{B \times C \times H \times W}$ contains complex-valued frequency coefficients.

To extract different frequency bands, we define two complementary radial binary masks:

$$\mathcal{M}_{\text{lf}} = \mathbb{I}(r < \rho), \quad \mathcal{M}_{\text{hf}} = 1 - \mathcal{M}_{\text{lf}}, \quad (2)$$

where r denotes the radial distance from the spectral center, and ρ is a predefined cutoff threshold.

We isolate the low- and high-frequency components by applying the masks element-wise:

$$\mathbf{X}_{\text{lf}} = \mathbf{X}_f \odot \mathcal{M}_{\text{lf}}, \quad \mathbf{X}_{\text{hf}} = \mathbf{X}_f \odot \mathcal{M}_{\text{hf}}, \quad (3)$$

where \odot denotes Hadamard (element-wise) multiplication.

Finally, we recover the spatial-domain representations via the inverse Fourier transform:

$$\widehat{\mathbf{X}}_{\text{lf}} = \mathcal{F}_{\text{DFT}}^{-1}(\mathbf{X}_{\text{lf}}), \quad \widehat{\mathbf{X}}_{\text{hf}} = \mathcal{F}_{\text{DFT}}^{-1}(\mathbf{X}_{\text{hf}}), \quad (4)$$

resulting in real-valued tensors $\widehat{\mathbf{X}}_{\text{lf}}, \widehat{\mathbf{X}}_{\text{hf}} \in \mathbb{R}^{B \times C \times H \times W}$ representing the low- and high-frequency spatial features, respectively. These components are subsequently passed to dedicated branches for frequency-specific refinement.

3.1.2 Frequency–Temporal Feature Modulation. To enhance frequency- and spatial-domain representations in a disentangled manner, FreqWeaver introduces three specialized branches, each responsible

for modeling a specific component of the feature spectrum: low-frequency (global structure), high-frequency (local detail), and spatial-domain semantics. These branches operate independently and produce complementary signals for subsequent fusion.

Low-Frequency Branch. This branch targets the restoration of global semantic coherence and suppression of large-scale distortions, which are commonly observed in low-frequency-dominated regions such as terrain or vegetation. By modeling long-range dependencies, it reinforces region-level consistency across the scene.

The low-frequency response is computed as:

$$\mathbf{F}_{\text{lf}} = \mathcal{F}_{\text{LF}}(\widehat{\mathbf{X}}_{\text{lf}}), \quad (5)$$

where $\widehat{\mathbf{X}}_{\text{lf}} \in \mathbb{R}^{B \times C \times H \times W}$ is the input low-frequency feature map, and $\mathcal{F}_{\text{LF}}(\cdot)$ denotes a depthwise convolution with a kernel size of 11×11 , initialized with zeros. The output $\mathbf{F}_{\text{lf}} \in \mathbb{R}^{B \times C \times H \times W}$ encodes coarse structural information and is reshaped to $\mathbb{R}^{B \times H \times W \times C}$.

High-Frequency Branch. This branch emphasizes fine-grained details such as edges, contours, and textures—high-frequency components that are essential for distinguishing man-made objects and detailed structures. It enhances boundary clarity and preserves local precision.

The high-frequency response is defined as:

$$\mathbf{F}_{\text{hf}} = \mathcal{F}_{\text{HF}}(\widehat{\mathbf{X}}_{\text{hf}}), \quad (6)$$

where $\widehat{\mathbf{X}}_{\text{hf}} \in \mathbb{R}^{B \times C \times H \times W}$ is the high-frequency input, and $\mathcal{F}_{\text{HF}}(\cdot)$ is a depthwise convolution with a 5×5 kernel. The output $\mathbf{F}_{\text{hf}} \in$

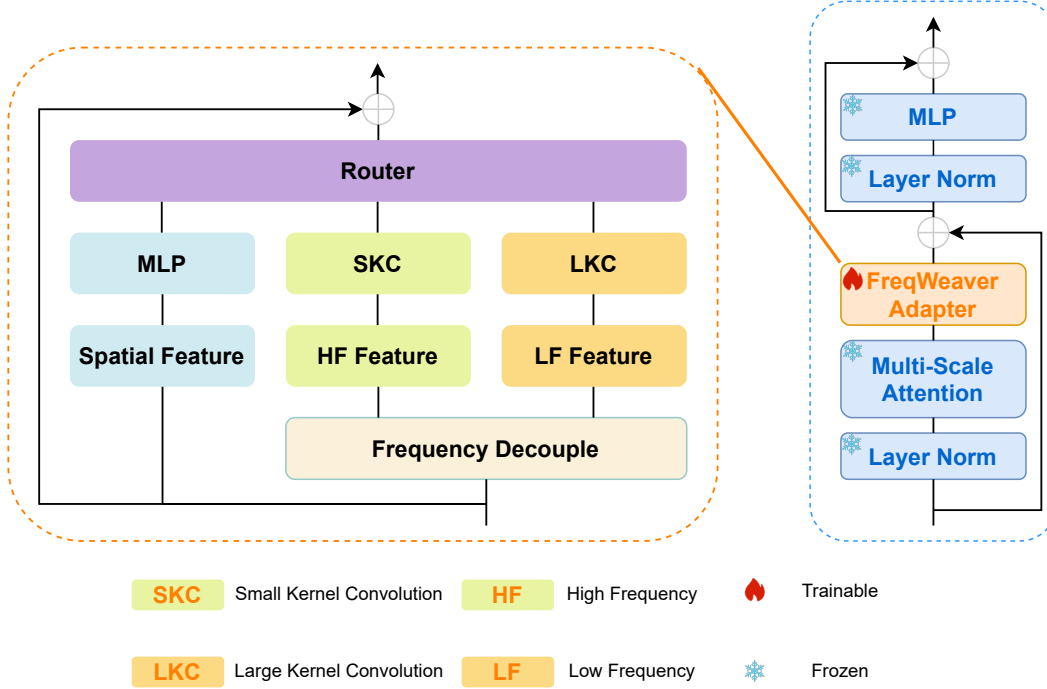


Figure 2: Overview of the proposed FreqWeaver Adapter.

$\mathbb{R}^{B \times C \times H \times W}$ highlights spatially localized structures and is similarly reshaped to $\mathbb{R}^{B \times H \times W \times C}$.

Spatial Branch. This branch directly processes the spatial-domain feature without spectral filtering, enabling the modeling of mid-frequency signals and ambiguous semantic cues that may not be cleanly separated in the frequency domain. It plays a complementary role in capturing transitional or occluded content.

The spatial-domain response is formulated as:

$$\mathbf{F}_s = \mathcal{F}_S(\mathbf{X}), \quad (7)$$

where $\mathbf{X} \in \mathbb{R}^{B \times H \times W \times C}$ is the original feature map before frequency decomposition. The operator $\mathcal{F}_S(\cdot)$ is a two-layer bottleneck MLP. The output $\mathbf{F}_s \in \mathbb{R}^{B \times H \times W \times C}$ captures spatial-domain semantics that complement the frequency-based branches.

3.1.3 Content-Aware Feature Fusion. To integrate the outputs of the frequency-temporal branches, we adopt a content-aware fusion strategy guided by global contextual information. This mechanism allows the model to dynamically balance the relative contributions of low-frequency, high-frequency, and spatial-domain features on a per-sample basis.

We first compute a global context descriptor via global average pooling over the spatial dimensions:

$$\mathbf{g} = \frac{1}{HW} \sum_{h=1}^H \sum_{w=1}^W \mathbf{X}_{:,h,w}, \in \mathbb{R}^{B \times C}, \quad (8)$$

where $\mathbf{X} \in \mathbb{R}^{B \times H \times W \times C}$ is the original spatial-domain feature map.

The descriptor \mathbf{g} is then passed to a lightweight router MLP, which outputs normalized fusion weights:

$$[r_s, r_{lf}, r_{hf}] = \text{softmax}(\mathcal{F}_{\text{Router}}(\mathbf{g})) \in \mathbb{R}^{B \times 3}, \quad (9)$$

where $\mathcal{F}_{\text{Router}}(\cdot)$ denotes a two-layer MLP with softmax normalization to ensure $\sum_k r_k = 1$.

Finally, the modulation outputs are adaptively fused with the original features via weighted addition:

$$\mathbf{Y} = \mathbf{X} + r_s \odot \mathbf{F}_s + r_{lf} \odot \mathbf{F}_{lf} + r_{hf} \odot \mathbf{F}_{hf}, \quad (10)$$

where \odot denotes broadcasted element-wise multiplication. The final output $\mathbf{Y} \in \mathbb{R}^{B \times H \times W \times C}$ preserves the original spatial resolution while incorporating frequency- and content-aware enhancements.

This fusion strategy enables adaptive emphasis of complementary information sources, thereby improving the model’s ability to generalize to diverse spatial patterns in remote sensing imagery.

3.2 Uncertainty-Aware Teacher-Student Adaptation

In the context of remote sensing segmentation, acquiring large-scale annotated datasets is both expensive and labor-intensive. To alleviate this constraint, we introduce an **Uncertainty-Aware Mean Teacher (UAMT)** framework that leverages unlabeled data via a dual-network consistency paradigm. The method enhances pseudo-supervision reliability by integrating entropy-based uncertainty

estimation into a perturbation-consistent learning scheme. This design allows for stable adaptation of large vision foundation models (e.g., SAM2) with minimal supervision.

3.2.1 Mean Teacher Framework with Perturbation Consistency. Our framework adopts a teacher-student architecture where the student network θ_S is optimized via gradient descent, while the teacher network θ_T acts as a temporal ensemble, updated using Exponential Moving Average (EMA) to ensure stable supervision:

$$\theta_T^{(t)} = \alpha \theta_T^{(t-1)} + (1 - \alpha) \theta_S^{(t)}, \quad \alpha = 0.99, \quad (11)$$

where α is the EMA decay coefficient controlling the momentum of the update.

To enforce robustness under data augmentation, each unlabeled input $x_u \in \mathcal{D}_u$ is subjected to two augmentation pipelines: a weakly augmented version $\tilde{x}_u^{\text{weak}}$ is fed to the teacher model, while a strongly augmented counterpart $\tilde{x}_u^{\text{strong}}$ is provided to the student. The underlying assumption is that semantic predictions should remain consistent across these perturbations, even if the appearance varies. Accordingly, consistency regularization is applied to align the outputs of teacher and student networks under this augmentation mismatch.

3.2.2 Entropy-Based Uncertainty Estimation. While teacher predictions provide valuable supervisory cues, pseudo-labels generated for remote sensing images are particularly error-prone due to complex backgrounds, fine-grained object boundaries, and domain-specific variations. To mitigate the impact of such noisy supervision, we employ a pixel-wise confidence estimation mechanism based on Shannon entropy to downweight uncertain predictions.

Let $\mathbf{P}_j^T \in \mathbb{R}^C$ denote the softmax probability vector predicted by the teacher at pixel j , where C is the number of classes. The uncertainty score is quantified by entropy:

$$\mathcal{H}_j = - \sum_{c=1}^C \mathbf{P}_{j,c}^T \log \mathbf{P}_{j,c}^T, \quad (12)$$

which attains its maximum at $\log C$ when the prediction is maximally ambiguous (i.e., uniform distribution). To normalize this measure and convert it into a usable confidence weight, we define:

$$w_j = 1 - \frac{\mathcal{H}_j}{\log C}, \quad w_j \in [0, 1], \quad (13)$$

where higher w_j values indicate more confident predictions and hence stronger training signals. This design enables the model to suppress the impact of high-entropy (uncertain) regions and focus on reliable pseudo-labels.

3.2.3 Loss Function: Supervised-Unsupervised Coupling. The overall objective consists of two complementary terms: a supervised loss on labeled data and a confidence-weighted consistency loss on unlabeled data.

Supervised Loss. Given labeled samples $(x_l, y_l) \in \mathcal{D}_l$, the student model is trained with standard pixel-wise cross-entropy:

$$\mathcal{L}_{\text{sup}} = \text{CE}(f(x_l; \theta_S), y_l), \quad (14)$$

where $f(\cdot; \theta_S)$ denotes the student prediction.

Consistency Loss with Confidence Weighting. For unlabeled images $x_u \in \mathcal{D}_u$, the teacher generates soft predictions \mathbf{P}^T , while the student predicts \mathbf{P}^S from a strongly perturbed view. A pseudo-label $\hat{y}_j^T = \arg \max_c \mathbf{P}_{j,c}^T$ is assigned per pixel, and the confidence-weighted consistency loss is formulated as:

$$\mathcal{L}_{\text{cons}} = \frac{1}{|\mathcal{D}_u| \cdot N} \sum_{x_u \in \mathcal{D}_u} \sum_{j=1}^N w_j \cdot \text{CE}(\mathbf{P}_j^S, \hat{y}_j^T), \quad (15)$$

where N is the total number of pixels per image, and \mathbf{P}_j^S is the predicted softmax from the student at pixel j .

Total Objective. The combined loss is given by:

$$\mathcal{L}_{\text{total}} = \mathcal{L}_{\text{sup}} + \lambda \cdot \mathcal{L}_{\text{cons}}, \quad (16)$$

where $\lambda = 0.1$ balances the contributions of labeled and unlabeled samples.

During training, only the parameters of the FreqWeaver adapters are updated, while the SAM2 backbone remains frozen. This strategy ensures efficient and stable transfer to remote sensing domains, leveraging both labeled and unlabeled data in a principled manner.

4 EXPERIMENT

4.1 Dataset

In this study, all experiments were conducted on ultra-high-resolution remote sensing imagery of Baltimore, captured at a spatial resolution of 0.3 meters. A total of 60 images, each with dimensions of 1024×1024 pixels, were selected based on the nine urban semantic categories defined by *UrbanWatch*, ensuring a relatively balanced distribution of class labels, as shown in Fig 4. The dataset comprises a total of 62,914,560 pixels. For initial annotations, we utilized the *UrbanWatch* model, which was originally trained on 1-meter resolution imagery. Although not optimized for ultra-high-resolution inputs, this model offered a coarse yet informative baseline. To improve annotation accuracy, we subsequently performed meticulous manual corrections. Given the complexity of remote sensing scenes and the difficulty of pixel-level labeling, this process was both labor-intensive and time-consuming. For training and evaluation, we used 55 images for training and the remaining 5 for testing. The test set alone contained 5,242,880 pixels, offering a sufficiently large sample size for robust and reliable performance evaluation.

4.2 Evaluation Metrics

To comprehensively evaluate the segmentation performance, we adopt two widely used metrics: Intersection over Union (IoU) and Dice coefficient. Both metrics quantify the region-level overlap between predicted segmentation results and ground truth annotations, providing a general assessment of segmentation accuracy.

Given the predicted region P and the ground truth region G , the IoU and Dice coefficient are defined as follows:

$$\text{IoU} = \frac{|P \cap G|}{|P \cup G|}, \quad (17)$$

$$\text{Dice} = \frac{2|P \cap G|}{|P| + |G|}, \quad (18)$$

where $|P \cap G|$ denotes the number of pixels in the intersection of the prediction and the ground truth, and $|P \cup G|$ denotes the number of

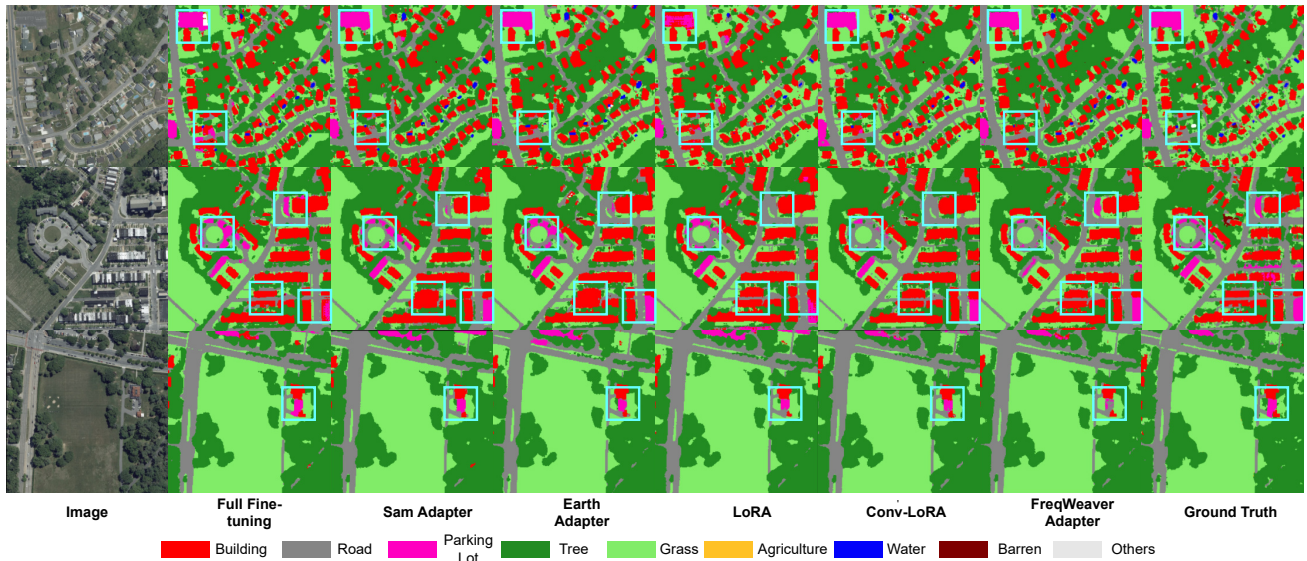


Figure 3: Visualization of the State-of-the-Art PEFT Method.

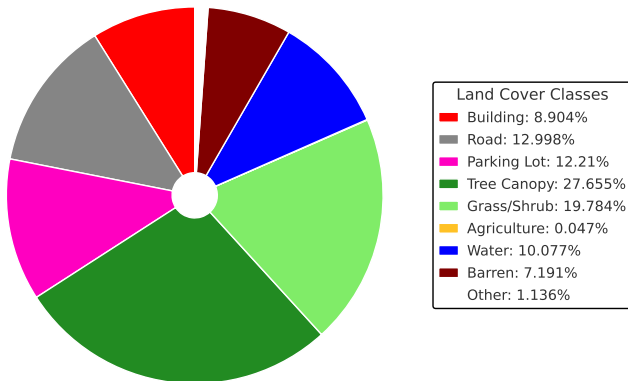


Figure 4: Visualization of land cover class distribution.

pixels in their union. Higher values of IoU and Dice indicate better segmentation performance.

4.3 Training and Testing Details

All experiments were conducted using PyTorch on a single NVIDIA RTX L40S GPU with 48 GB of memory. In our work, we adopt SAM2 as the backbone network. Input images were uniformly resized to 1024×1024 during both training and testing. The model was trained for 200 epochs using the Adam optimizer with a learning rate of 5×10^{-4} and a batch size of 2.

For the segmentation task, we employed the standard Cross-Entropy loss, placing emphasis on accurate pixel-wise classification as the primary optimization objective.

Table 1: Comparison with state-of-the-art parameter-efficient fine-tuning (PEFT) methods.

Methods	IoU	Dice	Param
Full Fine-tuning	0.5239	0.6006	69.11M
Earth Adapter (2025) [15]	0.5149	0.5893	10.19M
LoRA (2021) [11]	0.5202	0.5909	0.48M
SAM Adapter (2023) [45]	0.5321	0.6116	5.64M
Conv-LoRA (2024) [51]	0.5342	0.6051	0.50M
Ours	0.5520	0.6331	4.12M

4.4 Comparison With State-of-the-Art PEFT Methods

To evaluate the effectiveness of the proposed adapter, we conducted extensive comparative experiments against several state-of-the-art parameter-efficient fine-tuning (PEFT) methods, including the SAM Adapter[45], LoRA[11], Conv-LoRA[51], and the Earth Adapter[15]. These approaches represent diverse strategies for adapting large-scale models like SAM2, with different focuses on domain specificity and parameter efficiency, as summarized in Table 1.

Limitations of LoRA and Conv-LoRA. Our experimental results show that both LoRA and Conv-LoRA achieve competitive performance with remarkably low parameter overhead. LoRA, which leverages low-rank decomposition for efficient adaptation, is widely adopted for lightweight fine-tuning tasks. However, due to its linear structure, it exhibits limited capability in modeling the spatial complexity of high-resolution remote sensing scenes, which often involve multi-scale objects, intricate semantics, and fine-grained textures. To address this limitation, Conv-LoRA enhances the original LoRA design by incorporating convolutional

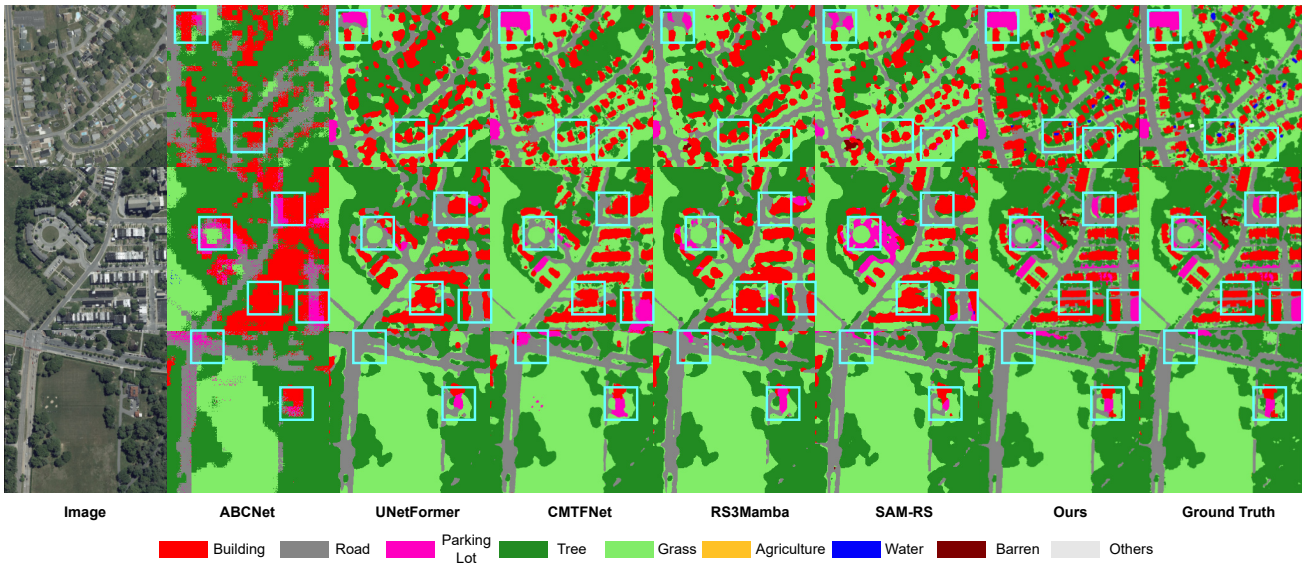


Figure 5: Visualization of the State-of-the-Art LULC Method.

layers to strengthen local feature extraction. This modification improves its ability to model small objects and boundary details, leading to noticeable performance gains. Nonetheless, despite these improvements, Conv-LoRA still lacks the representational capacity to fully exploit the potential of high-resolution remote sensing imagery, particularly in capturing complex spatial-frequency interactions, leaving room for further enhancement.

Limitations of Earth Adapter and SAM Adapter. The Earth Adapter, although specifically designed for remote sensing tasks, attempts to decouple frequency components without incorporating targeted spatial modeling mechanisms. This results in relatively high parameter consumption and unsatisfactory performance. The SAM Adapter, originally developed for medical image segmentation, shows moderate adaptability when transferred to remote sensing domains. However, due to the increased complexity and resolution of remote sensing data, it struggles to effectively model fine-grained structures and semantic variations.

Effectiveness of the Proposed FreqWeaver Adapter. In contrast, our proposed FreqWeaver Adapter introduces a frequency-aware design tailored for remote sensing applications. By explicitly decoupling low- and high-frequency components and applying targeted processing strategies to each, FreqWeaver effectively suppresses low-frequency artifacts while preserving high-frequency structural details. This leads to improved segmentation accuracy and better adaptation to the SAM2 backbone. Importantly, FreqWeaver achieves this superior performance with fewer parameters than both the Earth Adapter and the SAM Adapter, demonstrating its strong domain-specific effectiveness and efficiency for high-resolution remote sensing tasks. We also present visualizations to validate the effectiveness of our method, as shown in 3.

Table 2: Comparison with state-of-the-art Land Use and Land Cover (LULC) methods.

Methods	IoU	Dice
ABCNet(2021)[22]	0.4111	0.5217
UNetFormer(2022)[42]	0.5236	0.6201
CMTFNet(2023)[44]	0.5428	0.6369
RS ³ Mamba(2024)[28]	0.5092	0.6068
SAM-RS(2024)[27]	0.5434	0.6342
Ours	0.5778	0.6545

4.5 Comparison with State-of-the-Art Land Cover Classification Methods

To evaluate the effectiveness of our proposed approach, we conducted extensive comparative experiments against several representative state-of-the-art Land Cover and Land Use Classification (LULC) methods. Specifically, we selected five recent and competitive baselines from the literature (2021–2024)—ABCNet [22], UNetFormer [42], CMTFNet [44], RS³Mamba [28], and SAM-RS [27] chosen for their strong benchmark performance and representation of diverse architectural paradigms, including CNN-based, Transformer-based, and Mamba-based models. The quantitative comparison results are reported in Table 2, while qualitative visualization examples are provided in Fig. 5 to further illustrate the advantages of our method.

Limitations of Existing Methods. Quantitative results (Table 2) demonstrate that the proposed method consistently outperforms all selected baseline methods. In comparison to the strongest baseline, SAM-RS, our model achieves an improvement of 3.44% in IoU and 2.03% in Dice score, underscoring its superior performance

in LULC tasks. Despite the reasonable segmentation accuracy exhibited by prior methods, visual analysis reveals several limitations: (1) Misclassification remains prevalent in complex scenes, particularly those with high intra-class variance or subtle inter-class distinctions (e.g., differentiating various types of vegetation or urban structures); (2) Object boundaries are often rendered blurry and imprecise, a critical deficiency for ultra-high-resolution segmentation tasks that demand sharp delineations; (3) Models generally perform well on spectrally distinct classes like grass and trees, but falter with categories exhibiting complex geometries or semantic overlaps, such as distinguishing between parking lots and buildings, or between roads and barren land. Moreover, small object detection, such as identifying pools in residential areas, is often overlooked by existing approaches.

Effectiveness of Our Method. To the best of our knowledge, our model is the first to adapt the Segment Anything v2 (SAM2) architecture for the task of LULC. By leveraging the rich prior knowledge encoded in this foundation model, we obtain robust category- and pixel-level representations. Building upon this foundation, the proposed FreqWeaver Adapter enhances the semantic granularity of feature modeling—by explicitly capturing and integrating multi-frequency information crucial for detail preservation—thereby enabling significantly improved delineation of object boundaries and detection of small structures. Notably, the enhanced feature representation from the FreqWeaver Adapter allows our model to effectively exploit contextual cues, such as the presence or absence of vehicles, to better distinguish between semantically similar regions like parking lots and roads. These capabilities demonstrate the strengths of our architecture in ultra-high-resolution LULC tasks. Additionally, the integration of a semi-supervised learning strategy further improves the robustness and generalization of our model under limited annotation scenarios.

Table 3: Classification performance on ultra-high resolution Downstream Applications.

Class	User’s Accuracy (%)	Producer’s Accuracy (%)
Building	93.71	81.71
Road	85.39	89.94
Parking lot	85.00	85.53
Tree Canopy	75.58	98.98
Grass/Shrub	91.80	73.36
Agriculture	0.00	0.00
Water	94.92	98.25
Barren	80.00	40.00
Other	60.00	54.55
Overall Accuracy (OA)	84.55%	
Kappa Coefficient	81.38%	

4.6 Exploration of Downstream Applications in Map Analysis

To evaluate the practicality of our approach in real-world scenarios, we applied the proposed method to downstream ultra-high-resolution map analysis tasks, as summarized in Table 3. Despite being trained on a relatively small dataset, our method exhibits strong generalization capabilities, achieving an Overall Accuracy (OA) of 84.55% and a Kappa coefficient of 81.38%. These metrics

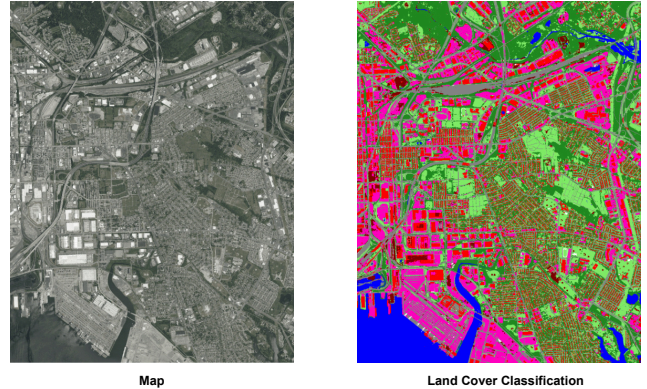


Figure 6: Visualization of Land Cover Classification.

reflect not only the correctness of predictions but also the statistical reliability of classification performance across diverse land cover categories.

A detailed breakdown of class-wise performance is provided in Table 3. Notably, high User’s Accuracy was achieved for categories such as *Building* (93.71%), *Water* (94.92%), and *Grass/Shrub* (91.80%), indicating precise identification of spatial regions with distinct spectral or structural characteristics. At the same time, balanced Producer’s Accuracy was maintained, particularly for *Tree Canopy* (98.98%) and *Road* (89.94%), demonstrating strong recall and comprehensive spatial coverage.

Nevertheless, certain challenges persist in distinguishing semantically overlapping or visually ambiguous regions, such as *Tree Canopy vs. Grass/Shrub* and *Parking Lot vs. Road*, which are frequently misclassified due to spatial proximity or similar textures.

To further validate the effectiveness of our method, qualitative visualizations were performed on real-world map segments, as illustrated in Fig. 6. The results show that our approach successfully preserves object boundaries, captures fine-grained structures, and adapts effectively to spatial heterogeneity, confirming its suitability for downstream high-resolution map analysis tasks.

Table 4: Quantitative results of the ablation study.

FW	UATS	IoU	Dice
✗	✗	0.5239	0.6006
✓	✗	0.5520	0.6331
✓	✓	0.5778	0.6545

4.7 Ablation Studies

To evaluate the contribution of each component within the proposed framework, we conducted extensive ablation studies, as shown in Table 4. In each experiment, specific modules—FreqWeaver (FW) and the Uncertainty-Aware Teacher Student Model (UATS)—were selectively enabled or disabled to analyze their individual impact on segmentation performance.

Effectiveness of FreqWeaver. We introduce FreqWeaver (FW) to decouple the frequency and temporal components within SAM2, enabling a parameter-efficient mechanism to capture complex patterns in remote sensing imagery. Experimental results show that, compared to full fine-tuning, our method achieves a 2.81% improvement in IoU and a 3.25% improvement in Dice score, while updating only 5.96% of the total parameters. These findings highlight the effectiveness of FreqWeaver in fine-tuning large vision models for remote sensing tasks and provide a scalable pathway for adapting foundation models under strict resource constraints.

Effectiveness of the Uncertainty-Aware Teacher-Student Model. We introduce the Uncertainty-Aware Teacher-Student model (UATS) to mitigate the impact of unreliable pseudo-labels, which are common in remote sensing imagery due to complex backgrounds and ambiguous boundaries. By incorporating uncertainty estimation into the consistency learning framework, UATS effectively downweights noisy supervision and makes better use of unlabeled data in the semi-supervised setting. As shown in our experiments, adding UATS on top of FreqWeaver leads to a 2.58% improvement in IoU and a 2.14% improvement in Dice score. These results demonstrate the importance of uncertainty modeling in enhancing model robustness and generalization across diverse remote sensing scenes.

Table 5: Quantitative results of the Adaptation ablation study.

Stage 1	Stage 2	Stage 3	Stage 4	IoU	Dice
✓	✓	✓	✓	0.5238	0.5997
✗	✓	✓	✓	0.4955	0.5694
✗	✗	✓	✓	0.5520	0.6331
✗	✗	✗	✓	0.3722	0.4633

4.8 Segment Anything 2 Adaptation

Segment Anything 2 is built upon the Hierarchical Detection Transformer (HieraDet), a multi-scale transformer architecture composed of four stages. In the original Segment Anything framework, adapters such as the SAM Adapter are inserted into every transformer block. However, directly applying this strategy to Segment Anything 2 often results in suboptimal fine-tuning performance due to its deeper and hierarchically structured design. To better accommodate these architectural differences, we conducted a series of empirical studies to investigate more effective adapter integration strategies. The results are presented in Table 5.

Specifically, we hypothesize that fine-tuning a foundation model to adapt to downstream tasks such as remote sensing segmentation primarily requires the adjustment of deeper semantic layers. Therefore, we initially inserted adapters into all four stages and gradually moved toward inserting them only in the deeper stages. Experimental results reveal that adding adapters to early transformer stages not only fails to improve domain adaptation, but can even hinder the model’s ability to specialize for remote sensing data. Conversely, limiting adapter placement to only the final stage also leads to underfitting, as the model lacks sufficient capacity for structural adaptation. We observe that inserting adapters into Stage 3 and Stage 4 yields the best performance, striking a balance

between semantic depth and structural flexibility. While our experiments primarily report results using the proposed FreqWeaver Adapter, we also validated this stage-wise trend using other adapter designs, including the SAM Adapter and Earth Adapter, and found consistent behavior across all cases.

5 CONCLUSION

In this work, we proposed a parameter-efficient semi-supervised segmentation framework for high-resolution remote sensing imagery. By integrating a domain-adaptive FreqWeaver Adapter with the SAM2 backbone and employing an uncertainty-aware teacher student strategy, our method addresses the challenges of limited annotations, scale variation, and structural consistency. Experiments show that our approach achieves strong segmentation performance with minimal parameter overhead, outperforming existing PEFT and high-resolution segmentation methods. These results highlight the potential of combining spectral decomposition and semi-supervised learning for effective foundation model adaptation in remote sensing.

6 DISCUSSION

One limitation of our current study lies in the geographic scope of the dataset, which is primarily extracted from selected regions within Baltimore City. Although class balancing techniques were applied during preprocessing, certain land cover categories—such as agriculture—remain significantly underrepresented. This imbalance may introduce bias into the model’s learning process, particularly in recognizing rare or sparsely distributed classes. In future work, we plan to extend our dataset to comprehensively cover the entire Baltimore City area. By doing so, we aim to achieve a more balanced and representative distribution of land cover classes, which is expected to enhance the generalizability and robustness of the segmentation model.

ACKNOWLEDGMENTS

This research is part of the funded project "BaltimoreAtlas: An ultra-high-resolution land cover and land use classification for the Greater Baltimore Metropolitan Area", supported by the School of Emerging Technologies (SET) seed funding, awarded by Towson University. Additional data acquisition, processing, and analysis were supported by the U.S. Geological Survey under Grant/Cooperative Agreement No. G23AP00683 (GY23-GY27).

REFERENCES

- [1] Xiaokang Chen, Yuhui Yuan, Gang Zeng, and Jingdong Wang. 2021. Semi-Supervised Semantic Segmentation with Cross Pseudo Supervision. arXiv:2106.01226.
- [2] Xiang Cheng and Hong Lei. 2023. Semantic Segmentation of Remote Sensing Imagery Based on Multiscale Deformable CNN and DenseCRF. *Remote Sens.* 15, 5 (2023), 1229.
- [3] Alexey Dosovitskiy, Lucas Beyer, Alexander Kolesnikov, Dirk Weissenborn, Xiaohua Zhai, Thomas Unterthiner, Mostafa Dehghani, Matthias Minderer, Georg Heigold, Sylvain Gelly, Jakob Uszkoreit, and Neil Houlsby. 2021. An Image is Worth 16x16 Words: Transformers for Image Recognition at Scale. arXiv:2010.11929.
- [4] Mingcen Fan and Mohan Zhou. 2025. Revisiting Consistency Regularization for Semi-Supervised Learning with Vision Foundation Models. arXiv:2503.09707.
- [5] Shengxi Gui, Shuang Song, Rongjun Qin, and Yang Tang. 2024. Remote Sensing Object Detection in the Deep Learning Era—A Review. *Remote Sens.* 16, 2 (2024), 327.

- [6] Tuo Guo, Xiaoyu Ma, Pengyuan Ren, Tian He, Rui Zhu, Jingnan Zhang, Fang Liu, Jiaqi Wang, Wenjia Wang, Wentong Li, and Dahua Lin. 2024. SkySense: A Multi-Modal Remote Sensing Foundation Model Towards Universal Interpretation. In *Proc. CVPR*. 27306–27317.
- [7] Zeyu Han, Chao Gao, Jinyang Liu, Jeff (Jun) Zhang, and Sai Qian Zhang. 2024. Parameter-Efficient Fine-Tuning for Large Models: A Comprehensive Survey. arXiv:2403.14608.
- [8] Haoyu He, Jianfei Cai, Jing Zhang, Dacheng Tao, and Bohan Zhuang. 2023. Sensitivity-Aware Visual Parameter-Efficient Fine-Tuning. In *Proc. ICCV*. 11825–11835.
- [9] Mingyuan He, Jie Zhang, Yang He, Xinjie Zuo, and Zebin Gao. 2024. Annotated Dataset for Training Cloud Segmentation Neural Networks Using High-Resolution Satellite Remote Sensing Imagery. *Remote Sens.* 16, 19 (2024), 3682.
- [10] Neil Houlsby and Andrei Giurgiu. 2019. Parameter-Efficient Transfer Learning for NLP. In *Proc. ICLR*. 2790–2799.
- [11] Edward J. Hu and Yelong Shen. 2022. LoRA: Low-Rank Adaptation of Large Language Models. In *Proc. ICLR*.
- [12] Edward J. Hu, Yelong Shen, Phillip Wallis, Zeyuan Allen-Zhu, Yuanzhi Li, Shean Wang, Lu Wang, and Weizhu Chen. 2021. LoRA: Low-Rank Adaptation of Large Language Models. arXiv:2106.09685.
- [13] Leiyei Hu, Wanxuan Lu, Hongfeng Yu, Dongshuo Yin, Xian Sun, and Kun Fu. 2024. TEA: A Training-Efficient Adapting Framework for Tuning Foundation Models in Remote Sensing. *IEEE Trans. Geosci. Remote Sens.* 62 (2024), 1–18.
- [14] Leiyei Hu, Hongfeng Yu, Wanxuan Lu, Dongshuo Yin, Xian Sun, and Kun Fu. 2024. AiRs: Adapter in Remote Sensing for Parameter-Efficient Transfer Learning. *IEEE Trans. Geosci. Remote Sens.* 62 (2024), 1–18.
- [15] Xiaoxing Hu, Ziyang Gong, Yupei Wang, Yuru Jia, Gen Luo, and Xue Yang. 2025. Earth-Adapter: Bridge the Geospatial Domain Gaps with Mixture of Frequency Adaptation. arXiv:2504.06220.
- [16] Wubiao Huang, Fei Deng, Haibing Liu, Mingtao Ding, and Qi Yao. 2025. Multiscale Semantic Segmentation of Remote Sensing Images Based on Edge Optimization. *IEEE Trans. Geosci. Remote Sens.* 63 (2025), 1–13.
- [17] Menglin Jia, Luming Tang, Bor-Chun Chen, Claire Cardie, Serge Belongie, Bharath Hariharan, and Ser-Nam Lim. 2022. Visual Prompt Tuning. arXiv:2203.12119.
- [18] Zhenghao Jiang, Biao Wang, Peng Zhang, Yanlan Wu, Zhiyuan Ye, and Hui Yang. 2025. Semantic Enhancement and Change Consistency Network for Semantic Change Detection in Remote Sensing Images. *Int. J. Digit. Earth* 18, 1 (2025), e2496790.
- [19] Samar Khanna and Medhanie Irgau. 2024. ExPLoRA: Parameter-Efficient Extended Pre-Training to Adapt Vision Transformers under Domain Shifts. arXiv:2406.10973.
- [20] Alexander Kirillov, Eric Mintun, and Nikhila Ravi. 2023. Segment Anything. In *Proc. ICCV*. 3892–3904.
- [21] Alexander Kirillov, Eric Mintun, Nikhila Ravi, Hanzi Mao, Chloe Rolland, Laura Gustafson, Tete Xiao, Spencer Whitehead, Alexander C. Berg, and Wan-Yen Lo. 2023. Segment Anything. In *Proc. ICCV*. 3879–3890.
- [22] Rui Li, Shunyi Zheng, Ce Zhang, Chenxi Duan, Libo Wang, and Peter M. Atkinson. 2021. ABCNet: Attentive Bilateral Contextual Network for Efficient Semantic Segmentation of Fine-Resolution Remotely Sensed Imagery. *ISPRS J. Photogramm. Remote Sens.* 181 (2021), 84–98.
- [23] Xiaoxiang Li, Cheng Cheng, Zhiyong Chen, and Manchun Li. 2024. Hierarchical partition of urban land-use units by unsupervised graph learning from high-resolution satellite images. *Int. J. Geogr. Inf. Sci.* (2024).
- [24] Xiang Lisa Li and Percy Liang. 2021. Prefix-Tuning: Optimizing Continuous Prompts for Generation. arXiv:2101.00190.
- [25] Yanan Liu and Libao Zhang. 2025. Confidence-Guided Joint Complementary Learning for Weakly Annotated Remote Sensing Object Segmentation. *IEEE Trans. Geosci. Remote Sens.* 64 (2025), 1–14.
- [26] Jinna Lv, Qi Shen, Mingzheng Lv, Yiran Li, Lei Shi, and Peiyang Zhang. 2023. Deep learning-based semantic segmentation of remote sensing images: a review. *Front. Ecol. Evol.* 11 (2023), 1201125.
- [27] Xianping Ma, Qianqian Wu, Xingyu Zhao, Xiaokang Zhang, Man-On Pun, and Bo Huang. 2024. SAM-Assisted Remote Sensing Imagery Semantic Segmentation With Object and Boundary Constraints. *IEEE Trans. Geosci. Remote Sens.* 62 (2024), 1–16.
- [28] Xianping Ma, Xiaokang Zhang, and Man-On Pun. 2024. RS3Mamba: Visual State Space Model for Remote Sensing Image Semantic Segmentation. *IEEE Geosci. Remote Sens. Lett.* 21 (2024), 1–5.
- [29] Yue Ma, Bowen Dong, Lin Sun, Donghui Zhang, Xiaoyan Wang, Jun Wang, and Xianfang Sun. 2025. Transform Dual-Branch Attention Net: Efficient Semantic Segmentation of Ultra-High-Resolution Remote Sensing Images. *Remote Sens.* 17, 3 (2025), 540.
- [30] Francesc Martí-Escofet, Benedikt Blumenstiel, Linus Scheibenreif, Paolo Fraccaro, and Konrad Schindler. 2025. Fine-Tune Smarter, Not Harder: Parameter-Efficient Fine-Tuning for Geospatial Foundation Models. arXiv:2504.17397.
- [31] Marcos Mendieta, Zitu Yang, Yaxing Chen, Ziqi Yang, Chen Chen, and Zheng Wu. 2024. Toward Real Ultra Image Segmentation: Leveraging Surrounding Context to Cultivate General Segmentation Model. In *Adv. Neural Inf. Process. Syst.*
- [32] Clay Foundation: Clay Foundation Model. 2024. Clay. Available at: <https://huggingface.co/made-with-clay/Clay>.
- [33] G. Placeholder, C. Author, et al. 2024. GeoChat: Grounded Large Vision-Language Model for Remote Sensing. In *Proc. CVPR*.
- [34] S. Placeholder, M. Author, et al. 2024. S2MAE: A Spatial-Spectral Pretraining Foundation Model for Spectral Remote Sensing Data. In *Proc. CVPR*.
- [35] S. Placeholder, S. Author, et al. 2024. SkySense: A Multi-Modal Remote Sensing Foundation Model Towards Universal Interpretation for Earth Observation Imagery. In *Proc. CVPR*.
- [36] Nikhila Ravi and Valentin Gabeur. 2024. SAM 2: Segment Anything in Images and Videos. arXiv:2408.00714.
- [37] Kihyuk Sohn and David Berthelot. 2020. FixMatch: Simplifying Semi-Supervised Learning with Consistency and Confidence. In *Adv. Neural Inf. Process. Syst.*
- [38] Vanja Stojnic and Konstantin Klemmer. 2025. Parameter-Efficient Fine-Tuning Unlocks High-Resolution Geospatial Foundation Models. arXiv:2504.17397.
- [39] Daniela Szwarzman, Sujit Roy, Paolo Fraccaro, Porsteinn Eli Gislason, Benedikt Blumenstiel, Rinki Ghosal, Pedro Henrique de Oliveira, Joao Lucas de Sousa Almeida, Rocco Sedona, Yanghui Kang, Srija Chakraborty, Sizhe Wang, Carlos Gomes, Ankur Kumar, Myscon Truong, Denys Godwin, Hyunho Lee, Chia-Yu Hsu, Ata Akbari Asanjan, Besart Mujeci, Disha Shidham, Trevor Keenan, Paulo Arevalo, Wenwen Li, Hamed Alemohammad, Pontus Olofsson, Christopher Hain, Robert Kennedy, Bianca Zadrozny, David Bell, Gabriele Cavallaro, Campbell Watson, Manil Maskey, Rahul Ramachandran, and Juan Bernabe Moreno. 2025. Prithvi-EO-2.0: A Versatile Multi-Temporal Foundation Model for Earth Observation Applications. arXiv:2412.02732.
- [40] Antti Tarvainen and Harri Valpola. 2018. Mean Teachers Are Better Role Models: Weight-Averaged Consistency Targets Improve Semi-Supervised Deep Learning Results. arXiv:1703.01780.
- [41] Thuan Than, Nhat-Anh Nguyen-Dang, Dung Nguyen, Salwa K. Al Khatib, Ahmed Elhagry, Hai Phan, Yihui He, Zhiqiang Shen, Marios Savvides, and Dang Huynh. 2025. Knowledge Consultation for Semi-Supervised Semantic Segmentation. arXiv:2503.10693.
- [42] Libo Wang, Rui Li, Ce Zhang, Shenghui Fang, Chenxi Duan, Xiaoliang Meng, and Peter M. Atkinson. 2022. UNetFormer: A UNet-Like Transformer for Efficient Semantic Segmentation of Remote Sensing Urban Scene Imagery. *ISPRS J. Photogramm. Remote Sens.* 190 (2022), 196–214.
- [43] Shanwen Wang, Xin Sun, Changrui Chen, Danfeng Hong, and Jungong Han. 2025. Semi-supervised Semantic Segmentation for Remote Sensing Images via Multi-scale Uncertainty Consistency and Cross-Teacher-Student Attention. arXiv:2501.10736.
- [44] Honglin Wu, Peng Huang, Min Zhang, Wenlong Tang, and Xinyu Yu. 2023. CMTFNet: CNN and Multiscale Transformer Fusion Network for Remote-Sensing Image Semantic Segmentation. *IEEE Trans. Geosci. Remote Sens.* 61 (2023), 1–12.
- [45] Junde Wu, Wei Ji, Yuanpei Liu, Huazhu Fu, Min Xu, Yanwu Xu, and Yueming Jin. 2023. Medical SAM Adapter: Adapting Segment Anything Model for Medical Image Segmentation. arXiv:2304.12620.
- [46] Zhitong Yan and Ziqi Yang. 2024. Towards Open-Vocabulary Remote Sensing Image Semantic Segmentation. arXiv:2412.19492.
- [47] Mengyuan Yang, Rui Yang, Min Wang, Haiyan Xu, and Gang Xu. 2025. Integrating Unsupervised Domain Adaptation and SAM Technologies for Image Semantic Segmentation: A Case Study on Building Extraction from High-Resolution Remote Sensing Images. *Int. J. Digit. Earth* 18, 1 (2025), e2491108.
- [48] Jie Zhang, Yunxin Li, Xubing Yang, Rui Jiang, and Li Zhang. 2025. RSAM-Seg: A SAM-Based Model with Prior Knowledge Integration for Remote Sensing Image Semantic Segmentation. *Remote Sens.* 17, 4 (2025), 590.
- [49] Tong Zhang, Yin Zhuang, and Liang Chen. 2024. Consistency Regularization based on Masked Image Modeling for Semi-Supervised Remote Sensing Semantic Segmentation. *IEEE J. Sel. Top. Appl. Earth Obs. Remote Sens.* 17 (2024), 10713–10733.
- [50] Yindan Zhang, Gang Chen, Soe W. Myint, Yuyu Zhou, Geoffrey J. Hay, Jelena Vukomanovic, and Ross K. Meentemeyer. 2022. UrbanWatch: A 1-Meter Resolution Land Cover and Land Use Database for 22 Major Cities in the United States. *Remote Sens. Environ.* 278 (2022), 113106.
- [51] Zihan Zhong, Zhiqiang Tang, Tong He, Haoyang Fang, and Chun Yuan. 2024. Convolution Meets LoRA: Parameter Efficient Finetuning for Segment Anything Model. arXiv:2401.17868.

Received 20 February 2007; revised 12 March 2009; accepted 5 June 2009